A Minimal Seesaw Model For Neutrino Masses and the Origin of Matter

Débora Marques Barreiros
Under Supervision of Filipe Joaquim and Ricardo González Felipe
Centro de Física Teórica de Parículas, Instituto Superior Técnico, Lisboa, Portugal
(Dated: November 2017)

Despite of its remarkable success, the Standard Model cannot explain the massive character of neutrinos and the present baryon asymmetry of the Universe. Seesaw models are commonly used to solve these two problems. These models predict heavy states associated to the mechanism of neutrino mass generation which are also responsible for the dynamical production of a baryon-asymmetry in the early Universe, through their out-of-equilibrium decay, in a process called leptogenesis. We discuss the minimal type I seesaw model constrained by the presence of two texture zeros in the Dirac neutrino mass matrix. We perform a thorough analysis on the compatibility of the possible textures with current neutrino data. Furthermore, implementing the viable texture-zero structures in the leptogenesis framework, we conclude that the model predicts the right baryon asymmetry for temperatures of the order of 10^{13} to 10^{15} GeV.

Keywords: Baryon Asymmetry of the Universe; Leptogenesis; Neutrino masses; Neutrino Physics; Seesaw Mechanism; Texture Zeros.

I. Introduction

The Standard Model (SM) of particle physics is one of the most successful theories in modern theoretical and experimental physics, giving a remarkable insight into the fundamental structure of matter. However, it does not explain the complete picture. One of the unanswered questions is the mechanism which generates neutrinos masses. The seesaw mechanism is one of the most attractive explanations for this problem. In this thesis we study the minimal type I seesaw mechanism in the presence of texture zeros in the generated mass matrix for neutrinos. The considered zeros restrict significantly the number of high-energy parameters in the model increasing its predictability at the observable energy scale. We perform a thorough analysis of all the possible two-zero textures in the neutrino Dirac mass matrix and study their compatibility with the most recent neutrino data. We discuss as well the more restrictive case where elements of the Dirac matrix are equal. But the study of neutrino mass models goes beyond the correct prediction of neutrino masses and mixings. In our case, the heavy particles added to the SM decouple at high energies in the early Universe. Their out-of-equilibrium decays at that stage, in a process called thermal leptogenesis, may be the key for explaining the present matter-antimatter asymmetry. We will also explore the phenomenological consequences for leptogenesis of the considered neutrino mass model and, ultimately, its compatibility with the present baryon asymmetry of the Universe (BAU).

II. Neutrinos in the Standard Model and Beyond

The SM is a quantum non-abelian gauge theory that describes the strong, weak and electromagnetic interactions. The SM Lagrangian is invariant under the local gauge symmetry group $G_{SM} = SU(3)_c \times SU(2)_L \times U(1)_Y$, where the subscripts c, L and Y denote colour, left-handness and weak hypercharge. In the SM, fermions are represented by left-handed (LH) and right-handed (RH) chiral eigenfunctions of the matrix γ_5. This chiral spinors constitute the smallest irreducible representation of the Lorentz group, thus being the perfect building blocks of the SM. The LH fields are weak isospin doublets, while the RH fields are assumed to be singlets under $SU(2)_L$. Note that neutrino fields do not have a RH component in the SM.

Focusing on the electroweak (EW) part of the SM we may write the following $SU(2)_L \times U(1)_Y$ invariant Lagrangian for this theory,

$$\mathcal{L}_{EW} = \mathcal{L}_{\text{gauge}} + \mathcal{L}_{\text{matter}} + \mathcal{L}_{\text{Higgs}} + \mathcal{L}_{\text{Yukawa}}, \quad (1)$$

where $\mathcal{L}_{\text{gauge}}$ contains the kinetic terms for gauge bosons, $\mathcal{L}_{\text{matter}}$ describes the dynamics of matter and their interactions with gauge fields, $\mathcal{L}_{\text{Higgs}}$ contains the potential that induces the symmetry breaking $SU(2)_L \times U(1)_Y \to U(1)_{\text{Q}}$ and the Higgs kinetic term, and finally $\mathcal{L}_{\text{Yukawa}}$ describes the Yukawa interactions between fermions and the Higgs doublet, responsible for the charged-fermions mass assignment after spontaneous symmetry breaking (SSB).

A. Lepton Masses in the SM

Within the SM framework, the Yukawa Lagrangian for leptons reads

$$\mathcal{L}_{\text{Yukawa}} = -\mathbf{Y}^{\ell}_{\alpha\beta}\overline{\ell_{\alpha L}}\Phi e_{\beta R} + \text{H.c.}\,, \quad (2)$$

where $\mathbf{Y}^{\ell}$ is the Yukawa coupling matrix for charged leptons. When the Higgs field (Φ) acquires a non-zero vacuum expectation value (VEV) $\langle\phi\rangle_0 = (0\,,\,v)^T$, with $v = 174.1$ GeV, after SSB, the charged leptons become massive with a Dirac mass matrix given by $\mathbf{M}^{\ell} \equiv v\mathbf{Y}^{\ell}$. Since no RH neutrinos are present in the SM, it is not possible to construct a Dirac mass term for neutrinos.

Because they are neutral particles, one could think that a Majorana mass term, constructed using the LH neutrinos, could generate neutrino masses. Such term for ν_L is written as

$$\mathcal{L}_{\rm L}^{\rm Maj} = -\frac{1}{2}\overline{\nu_{\alpha L}}(\mathbf{M_L})_{\alpha\beta}(\nu_{\beta L})^c + \text{H.c.}\,, \tag{3}$$

where $\mathbf{M_L}$ is a 3×3 complex and symmetric Majorana mass matrix. Taking a closer look at the above mass term, one can see that it is not invariant under a global $U(1)$ gauge symmetry, violating any charge (for instance, electrical charge or lepton number). Despite of being Lorentz invariant, the term in Eq. (3) is not invariant under the SM symmetries. As a consequence, a Majorana mass term cannot be constructed in the context of the SM (nor a Dirac mass term, as previously seen). For that reason, neutrinos are strictly massless in the SM. Consequently, the SM does not account for flavour mixing in the leptonic sector, in contrast with the quark sector where the mixing is given by the Cabibbo-Kobayashi-Maskawa (CKM) matrix [1, 2]. This can be demonstrated by writing the lepton charged-current (CC) Lagrangian in the charged-lepton mass basis (using $\mathbf{U_L^{\ell\dagger}M^\ell U_R^\ell} = \text{diag}(m_e, m_\mu, m_\tau) \equiv \mathbf{d}^\ell$, where $\mathbf{U_{L,R}^\ell}$ are unitary matrices), and verifying that it remains diagonal in flavour. Thus, the leptonic sector of the SM is completely described by the three charged-lepton masses.

B. Neutrino Masses

The experimental evidence for neutrino flavour oscillations [3, 4], proves the massive character of neutrinos and the existence of flavour mixing in the leptonic sector. Thus, a mechanism for the generation of small neutrino masses, beyond the SM, must be constructed. We may adress this problem by taking a closer look at the Majorana mass term presented in Eq. (3). Although this term is not invariant under G_{SM}, it may be percieved as a low-energy trace left by a high-energy theory, described by a non-renormalisable term, which is itself invariant under the SM symmetries. The lowest dimension term that we are able to construct with the SM particle content is the so-called Weinberg operator [5] given by

$$\mathcal{L}_5 = \frac{\mathbf{c}_{\alpha\beta}}{\mathcal{M}}\overline{(\ell_{L\alpha})^c}\tilde{\Phi}^*\tilde{\Phi}^\dagger\ell_{L\beta} + \text{H.c.}\,, \tag{4}$$

where $\mathbf{c}$ is a dimensionless coupling matrix, $\mathcal{M}$ is a constant mass scale and $\tilde{\Phi} = i\tau_2\Phi$. As required, the operator in Eq. (4) reproduces successfully the mass term in Eq. (3) when the Higgs doublet acquires a VEV. Thus, after SSB, the effective low-energy operator reads

$$\mathcal{L}_5 \xrightarrow{SSB} -\frac{1}{2}\frac{v^2}{\mathcal{M}}\mathbf{c}_{\alpha\beta}\overline{(\nu_{L\alpha})^c}\nu_{L\beta} + \text{H.c.}\,. \tag{5}$$

Comparing the above result with Eq. (3), we may identify the coefficient $(v^2/\mathcal{M})\mathbf{c}$ with the Majorana mass for LH neutrinos $\mathbf{M_L^*}$. The higher the mass scale $\mathcal{M}$ is, the more suppressed are the effects of the $\mathcal{L}_5$ operator at the SM energies. A possible realisation of the high-energy operator is the seesaw mechanism. It occurs when we associate the mass scale $\mathcal{M}$ with the mass of a heavy particle (boson or fermion), with $\mathcal{M} \gg v^2$, which mediates the interaction of Eq. (4) at high energies. If the mass scale is high enough, neutrino masses become naturally smaller than the fermion masses proportional to v. According with the type of particle that is added to the SM, we get three main types of seesaw models: type I , type II or type III where the exchanged particles are heavy-fermion singlets (ν_R) under all the SM symmetries, triplet scalars (Δ) under $SU(2)_L$ or triplet fermions (Σ_R) under $SU(2)_L$, respectively.

We will discuss the type I sessaw mechanism hereafter. In this model, n_R RH neutrinos are added to the particle content of the SM (without any other assumption), grouped as $\nu_R = (\nu_{1R}, \nu_{2R}, ..., \nu_{n_RR})^T$. The most general gauge invariant and renormalisable Lagrangian for RH neutrinos in the type I seesaw model reads [6]

$$\begin{aligned}\mathcal{L}_{\nu_R} =& i\overline{\nu_R}\gamma^\mu\partial_\mu\nu_R - \\ &- \left[\overline{\ell_L}\tilde{\phi}\mathbf{Y}^\nu\nu_R + \frac{1}{2}\overline{(\nu_R)^c}\mathbf{M_R}\nu_R + \text{H.c.}\right]\,,\end{aligned} \tag{6}$$

where $\mathbf{Y}^\nu$ is a general complex $3\times n_R$ Yukawa matrix and $\mathbf{M_R}$ is a symmetric $n_R\times n_R$ Majorana mass matrix. The above Lagrangian may be written in the mass basis of the RH neutrinos, using

$$\begin{aligned}\nu_{sR} &\to (\mathbf{U_R})_{si}N_{iR},\\ \mathbf{U_R^T M_R U_R} &= \text{diag}(M_1, M_2, ..., M_{n_R}) \equiv \mathbf{d_M},\end{aligned} \tag{7}$$

where s and i are flavour and mass indices, respectively, and the Majorana mass eigenstates may then be defined as $(N_i)^c = N_i \equiv N_{iR} + (N_{iR})^c$. The N_i fields may be integrated out from the resultant Lagrangian, considering that their masses are much larger than the masses of the lepton and Higgs doublets in Eq. (6), and one gets the effective mass term

$$-\frac{1}{2}\overline{\ell_{\alpha L}}\tilde{\phi}\left(-\mathbf{Y}^\nu{\mathbf{M_R}}^{-1}\mathbf{Y}^{\nu T}\right)_{\alpha\beta}\tilde{\phi}^T(\ell_{\beta L})^c + \text{H.c.}\,. \tag{8}$$

The above expression corresponds to the operator in Eq. (4) with a coefficient given by the expression in parentheses. After SSB, the Lagrangian in Eq. (8) becomes

$$\mathcal{L}_{\rm I}^\nu = -\frac{1}{2}\overline{\nu_{\alpha L}}\mathbf{M}^\nu_{\alpha\beta}(\nu_{\beta L})^c + \text{H.c.}\,, \tag{9}$$

with the effective type I seesaw matrix for light neutrinos given by

$$\mathbf{M}^\nu \simeq -v^2\mathbf{Y}^\nu\mathbf{M_R^{-1}}\mathbf{Y}^{\nu T}\,. \tag{10}$$

From Eq. (10) one sees that the light-neutrino masses are quadratic in $v\mathbf{Y}^\nu$ and inversely proportional to $\mathbf{M_R}$, be-

ing naturally suppressed for very heavy sterile neutrinos. Note that $\mathbf{M}^\nu$ is a 3×3 complex matrix, diagonalised by the unitary matrix $\mathbf{U}^\nu$ as

$$\mathbf{U}^{\nu\,T}\mathbf{M}^\nu\mathbf{U}^\nu = \mathrm{diag}(m_1, m_2, m_3) = \mathbf{d_m}\,, \qquad (11)$$

where m_i are the real and positive masses of light-neutrinos ν_i. If neutrinos have a mass term, a mixing in the leptonic sector will arise. In the mass basis of charged leptons and light neutrinos, the CC Lagrangian is not diagonal and can be written as

$$\mathcal{L}^\ell_{CC} = -\frac{g}{\sqrt{2}}\overline{e'_L}\,\mathbf{U}\,\gamma^\mu\nu'_L W^-_\mu \;+\; \mathrm{H.c.}\,, \qquad (12)$$

with $\mathbf{U} = \mathbf{U_L^\ell}^\dagger\mathbf{U}^\nu$ being the so-called Pontecorvo-Maki-Nakagawa-Sakata (PMNS) matrix [7, 8] that parametrises lepton mixing. For three lepton families the PMNS matrix is parametrised by [9]

$$\mathbf{U} = \begin{pmatrix} c_{12}c_{13} & s_{12}c_{13} & s_{13}e^{-i\delta} \\ -s_{12}c_{23} - c_{12}s_{23}s_{13}e^{i\delta} & c_{12}c_{23} - s_{12}s_{23}s_{13}e^{i\delta} & s_{23}c_{13} \\ s_{12}s_{23} - c_{12}c_{23}s_{13}e^{i\delta} & -c_{12}s_{23} - s_{12}c_{23}s_{13}e^{i\delta} & c_{23}c_{13} \end{pmatrix} \begin{pmatrix} 1 & 0 & 0 \\ 0 & e^{i\alpha_{21}/2} & 0 \\ 0 & 0 & e^{i\alpha_{31}/2} \end{pmatrix}, \qquad (13)$$

where α_{21}, $\alpha_{31} \in [0, 2\pi[$ denote the two Majorana phases, $\delta \in [0, 2\pi[$ is the Dirac phase and $\theta_{ij} \in [0, \pi/2]$ are the three leptonic mixing angles.

Because the effective neutrino mass matrix is the low-energy manifestation of the high-energy seesaw model, it contains information about all low-energy observables. Only six of these quantities were experimentally measured from neutrino oscillation experiments: two neutrino mass-squared differences Δm^2_{21} and Δm^2_{31}, defined as $\Delta m^2_{ij} = m^2_i - m^2_j$, three mixing angles and the phase δ. The results obtained in the global analysis of neutrino data in the framework of three-neutrino oscillations, dated from November 2016 [10], are presented in Table I. The current data is consistent with an hierarchy among neutrino masses mass-squared differences characterised by the ratio $\Delta m^2_{21}/\Delta m^2_{31} \simeq \pm0.03$. Once the sign of Δm^2_{31} is still unknown, one may have two distinct mass orderings: the normal ordering (NO), where $m_1 < m_2 < m_3$, or the inverted ordering (IO), with $m_3 < m_1 < m_2$. In terms of the mass of the lightest neutrino, one has

$$\begin{aligned} \text{NO:}\quad & m_2 = \sqrt{m_1^2 + \Delta m^2_{21}}, \\ & m_3 = \sqrt{m_1^2 + |\Delta m^2_{31}|}, \\ \text{IO:}\quad & m_1 = \sqrt{m_3^2 + |\Delta m^2_{31}|}, \\ & m_2 = \sqrt{m_3^2 + |\Delta m^2_{31}| + \Delta m^2_{21}}. \end{aligned} \qquad (14)$$

In this thesis, we will consider a model in which the mass of the lightest neutrino is zero. Thus, two possible hierarchical mass spectra are possible: normal hierarchy (NH) with $0 \ll m_2 \ll m_3$, and inverted hierarchy (IH) with $0 \ll m_1 \lesssim m_2$.

In the type I seesaw mechanism the number of free parameters is quite large, when compared to the number of physical parameters at low energies. In the presence of n_R RH neutrinos, the Majorana sector, after diagonalisation of $\mathbf{M_R}$, has n_R free parameters, corresponding to the heavy-neutrino masses. In the basis where both $\mathbf{M_R}$ and $\mathbf{Y}^\ell$ are diagonal, the Yukawa sector, represented by the complex and arbitrary $3\times n_R$ matrix $\mathbf{Y}^\nu$ has $2\times3n_R$ real parameters ($3n_R$ phases + $3n_R$ moduli). If we perform a redefinition of the LH lepton doublets, three phases can be removed and we are left with $3(n_R-1)$ phases. Therefore, we end up with a total of $n_R + 3n_R + 3(n_R-1) = 7n_R - 3$ free parameters: $4n_R$ moduli and $3(n_R-1)$ phases. For $n_R = 3$ ($n_R = 2$) the model is described by 15 (11) effective parameters to be compared with 9 (7) low-energy parameters, leading to 6 (2) unknown real parameters.

Due to the large number of unknown (and yet inaccessible) parameters of seesaw models, the need of parametrising them arises. An example of that is the so-called Casas-Ibarra [11] parametrisation of the neutrino Yukawa matrix, given by

$$\mathbf{Y}^\nu = v^{-1}\mathbf{U_L^\ell}^*\mathbf{U}^*\,\mathbf{d_m^{1/2}}\,\mathbf{R}\,\mathbf{d_M^{1/2}}\,\mathbf{U_R^\dagger}\,, \qquad (15)$$

with $\mathbf{R}$ being a $3\times n_R$ complex and orthogonal matrix where the unknown parameters of the type I seesaw are encoded. For $n_R = 2$, the $\mathbf{R}$ matrix is parametrised with a single complex angle [11], corresponding to the effective unknown high-energy parameter.

Parameter	**Global Fit Results** 1σ $\{3\sigma\}$	
	Normal Ordering	Inverted Ordering
θ_{12} (°)	$33.56^{+0.77}_{-0.75}\{^{2.43}_{-2.18}\}$	
θ_{23} (°)	$41.6^{+1.5}_{-1.2}\{^{+11.2}_{-3,2}\}$	$50.0^{+1.1}_{-1.4}\{^{+3.1}_{-11.2}\}$
θ_{13} (°)	$8.46^{+0.15}_{-0.15}\{^{+0.44}_{-0.47}\}$	$8.49^{+0.15}_{-0.15}\{^{+0.44}_{-0.46}\}$
δ (°)	$261^{+51}_{-59}\{^{+99}_{-261}\}$	$277^{+40}_{-46}\{^{+114}_{-132}\}$
Δm^2_{21}	$7.50^{+0.19}_{-0.17}\{^{+0.59}_{-0.47}\}$	
Δm^2_{31}	$+2.524^{+0.040}_{-0.039}\{^{+0.119}_{-0.117}\}$	$-2.514^{+0.038}_{-0.041}\{^{+0.121}_{-0.115}\}$

Table I. Three-flavour oscillation parameters from the global fit [10] for both NO and IO. Δm^2_{21} and Δm^2_{31} are presented in units of 10^{-5} eV^2 and 10^{-3} eV^2, respectively.

III. Two-zero Neutrino Textures in the Minimal Type I Seesaw Model

Since two mass-squared differences were measured in neutrino oscillations, a type I seesaw model with a single RH neutrino is automatically excluded since it would imply the presence of two massless neutrinos. Hence, the two RH neutrino (2RHN) model is the minimal viable model. This is a quite economical way of addressing the neutrino mass problem. Since the number of high-energy parameters in this model is fairly reduced in comparison with other seesaw models, its predictability increases. In the 2RHN mass model, $n_R = 2$ in Eq. (6), and $\mathbf{Y}^\nu$ and $\mathbf{M_R}$ are reduced to 3×2 and 2×2 matrices, respectively. Because $\mathbf{M_R}$ becomes a rank-two matrix, the diagonalisation of the effective neutrino mass matrix in Eq. (10) results in a zero mass eigenvalue for the light neutrinos. Thus, the lightest neutrino must be massless and, consequently, its associated Majorana phase vanishes. Thus, we set $\alpha_{31} = 0$ and $\alpha \equiv \alpha_{21}$ in Eq. (13) henceforth. Additionally, there are only two neutrino mass spectra allowed in this model: NH with $m_1 = 0$, and IH with $m_3 = 0$ [see Eq. (14)].

The model is thus described by 11 free parameters, corresponding to 2 Majorana masses and 9 real parameters which specify $\mathbf{Y}^\nu$. Of these, only 2 are unknown, since 7 are determined by low-energy quantities, namely 2 non-zero neutrino masses, 3 mixing angles, a Dirac phase and a Majorana phase. Adopting the Casas-Ibarra parametrisation in Eq. (15), these two parameters may be encoded in the matrix $\mathbf{R}$, given by

$$\mathbf{R}_{\rm NH} = \begin{pmatrix} 0 & 0 \\ \cos z & -\sin z \\ \xi\sin z & \xi\cos z \end{pmatrix}, \; \mathbf{R}_{\rm IH} = \begin{pmatrix} \cos z & -\sin z \\ \xi\sin z & \xi\cos z \\ 0 & 0 \end{pmatrix}, \tag{16}$$

where z is a complex angle and $\xi = \pm1$ accounts for possible matrix reflections. Having a parametrisation for $\mathbf{R}$, one may replace it in Eq. (15) and the following expressions, for $\mathbf{Y}^\nu$ in the mass basis of charged leptons and RH neutrinos (Mass Basis), are obtained

$$\begin{aligned} (\mathbf{Y}^\nu_{\rm MB})_{\alpha1} &= \tfrac{\sqrt{M_1}}{v}\left(+\sqrt{m_2}\mathbf{U}^*_{\alpha2}\cos z \pm \sqrt{m_3}\mathbf{U}^*_{\alpha3}\sin z\right), \\ (\mathbf{Y}^\nu_{\rm MB})_{\alpha2} &= \tfrac{\sqrt{M_2}}{v}\left(-\sqrt{m_2}\mathbf{U}^*_{\alpha2}\sin z \pm \sqrt{m_3}\mathbf{U}^*_{\alpha3}\cos z\right), \end{aligned} \tag{17}$$

for NH and

$$\begin{aligned} (\mathbf{Y}^\nu_{\rm MB})_{\alpha1} &= \tfrac{\sqrt{M_1}}{v}\left(+\sqrt{m_1}\mathbf{U}^*_{\alpha1}\cos z \pm \sqrt{m_2}\mathbf{U}^*_{\alpha2}\sin z\right), \\ (\mathbf{Y}^\nu_{\rm MB})_{\alpha2} &= \tfrac{\sqrt{M_2}}{v}\left(-\sqrt{m_1}\mathbf{U}^*_{\alpha1}\sin z \pm \sqrt{m_2}\mathbf{U}^*_{\alpha2}\cos z\right), \end{aligned} \tag{18}$$

for IH. We are also interested in analysing the predictions from the 2RHN model for non-diagonal $\mathbf{M_R}$ and (or) $\mathbf{Y}^\ell$. In the latter cases, we will consider non-diagonal structures of $\mathbf{Y}^\ell$ whose predictions may be easily inferred trough trivial rotations of the diagonal case. Thus, one needs to generalise the obtained expressions for $\mathbf{Y}^\nu_{\rm MB}$ only for the case where $\mathbf{U_R}$ is no longer the identity (while $\mathbf{UL}^\ell = \mathbb{1}$). Recalling Eq. (15), one has

$$\mathbf{Y}^\nu_{\alpha i} = (\mathbf{Y}^\nu_{\rm MB})_{\alpha1}(\mathbf{U_R})^*_{i1} + (\mathbf{Y}^\nu_{\rm MB})_{\alpha2}(\mathbf{U_R})^*_{i2}\,. \tag{19}$$

Taking a closer look at the above expressions, it is clear that if we set an element of $\mathbf{Y}^\nu$ to zero, relations among the high and low-energy parameters will emerge. Moreover, requiring the existence of two zeros, relations among the mixing angles, neutrino masses and low-energy phases arise. Imposing such constraints in the model, which may be a consequence of hidden symmetries in the leptonic sector, is indeed a powerful tool that can be used to predicted unmeasured low-energy quantities.

NH	$\mathbf{Y}^\nu_{\alpha1} = 0$	$\mathbf{Y}^\nu_{\alpha2} = 0$
R_1	$-\xi\sqrt{\frac{m_2}{m_3}}\frac{\mathbf{U}^*_{\alpha2}}{\mathbf{U}^*_{\alpha3}}$	$\xi\sqrt{\frac{m_3}{m_2}}\frac{\mathbf{U}^*_{\alpha3}}{\mathbf{U}^*_{\alpha2}}$
R_2	i	$\frac{-i\sqrt{m_2}M_1\mathbf{U}^*_{\alpha2} + \xi\sqrt{m_3}M_2\mathbf{U}^*_{\alpha3}}{\sqrt{m_2}M_2\mathbf{U}^*_{\alpha2} + i\xi\sqrt{m_3}M_1\mathbf{U}^*_{\alpha3}}$
R_3	$\frac{i\sqrt{m_2}M_1\mathbf{U}^*_{\alpha2} + \xi\sqrt{m_3}M_2\mathbf{U}^*_{\alpha3}}{\sqrt{m_2}M_2\mathbf{U}^*_{\alpha2} - i\xi\sqrt{m_3}M_1\mathbf{U}^*_{\alpha3}}$	$-i$
R_4	i	$-i$
IH	$\mathbf{Y}^\nu_{\alpha1} = 0$	$\mathbf{Y}^\nu_{\alpha2} = 0$
R_1	$-\xi\sqrt{\frac{m_1}{m_2}}\frac{\mathbf{U}^*_{\alpha1}}{\mathbf{U}^*_{\alpha2}}$	$\xi\sqrt{\frac{m_2}{m_1}}\frac{\mathbf{U}^*_{\alpha2}}{\mathbf{U}^*_{\alpha1}}$
R_2	i	$\frac{-i\sqrt{m_1}M_1\mathbf{U}^*_{\alpha1} + \xi\sqrt{m_2}M_2\mathbf{U}^*_{\alpha2}}{\sqrt{m_1}M_2\mathbf{U}^*_{\alpha1} + i\xi\sqrt{m_2}M_1\mathbf{U}^*_{\alpha2}}$
R_3	$\frac{i\sqrt{m_1}M_1\mathbf{U}^*_{\alpha1} + \xi\sqrt{m_2}M_2\mathbf{U}^*_{\alpha2}}{\sqrt{m_1}M_2\mathbf{U}^*_{\alpha1} - i\xi\sqrt{m_2}M_1\mathbf{U}^*_{\alpha2}}$	i
R_4	i	$-i$

Table II. Expressions for $\tan z$ as a function of the low-energy parameters and the heavy-neutrino masses M_1 and M_2, for each texture and for NH and IH.

A. One and Two-zero textures in the 2RHN model

Nowadays, all the mixing angles and mass squared differences are well measured, so we will focus on extracting predictions for δ and α from our model. Requiring the presence of a single texture zero in $\mathbf{Y}^\nu$ [see Eq. (19)], we obtain expressions for the high-energy parameter z acoording to the six possible zero positions and the considered neutrino hierarchy. In this work we focus on matrices $\mathbf{M_R}$ with one or more zeros. The considered patterns may be identified as

$$\begin{aligned} R_1 &: \begin{pmatrix} \times & 0 \\ 0 & \times \end{pmatrix}, \; R_2 : \begin{pmatrix} 0 & \times \\ \times & \times \end{pmatrix}, \\ R_3 &: \begin{pmatrix} \times & \times \\ \times & 0 \end{pmatrix}, \; R_4 : \begin{pmatrix} 0 & \times \\ \times & 0 \end{pmatrix}, \end{aligned} \tag{20}$$

where $\times$ denotes a non-zero matrix element. In all cases, it is possible to rephase the RH fields such that $\mathbf{M_R}$ becomes real. Replacing the $\mathbf{U_R}$ matrix elements in Eq. (19), we obtain the expressions for $\tan z$ presented

in Table II.

A more restrictive model is obtained if we impose two simultaneous texture zeros. In particular, such constraints allow for the determination of the CP-violating phases, δ and α. In the 2RHN model, $\mathbf{Y}^\nu$ is a 3×2 matrix and hence fifteen different patters of two-zero textures are possible. Adopting the notation of [12], where three groups A, B and C are used to classify the possible $\mathbf{Y}^\nu$ structures, one has

$$A_1:\begin{pmatrix}0&0\\ \times&\times\\ \times&\times\end{pmatrix},\ A_2:\begin{pmatrix}\times&\times\\ 0&0\\ \times&\times\end{pmatrix},\ A_3:\begin{pmatrix}\times&\times\\ \times&\times\\ 0&0\end{pmatrix}. \quad (21)$$

These three structures are automatically excluded because they lead to two vanishing mixing angles [one of the light neutrinos would be decoupled from the Yukawa interaction in Eq. (6)]. Furthermore, in group B one has

$$\begin{aligned} &B_1:\begin{pmatrix}0&\times\\ \times&0\\ \times&\times\end{pmatrix},\ B_2:\begin{pmatrix}0&\times\\ \times&\times\\ \times&0\end{pmatrix},\ B_3:\begin{pmatrix}\times&\times\\ 0&\times\\ \times&0\end{pmatrix},\\ &B_4:\begin{pmatrix}\times&0\\ 0&\times\\ \times&\times\end{pmatrix},\ B_5:\begin{pmatrix}\times&0\\ \times&\times\\ 0&\times\end{pmatrix},\ B_6:\begin{pmatrix}\times&\times\\ \times&0\\ 0&\times\end{pmatrix}, \end{aligned} \quad (22)$$

and group C contains the textures

$$\begin{aligned} &C_1:\begin{pmatrix}0&\times\\ 0&\times\\ \times&\times\end{pmatrix},\ C_2:\begin{pmatrix}0&\times\\ \times&\times\\ 0&\times\end{pmatrix},\ C_3:\begin{pmatrix}\times&\times\\ 0&\times\\ 0&\times\end{pmatrix},\\ &C_4:\begin{pmatrix}\times&0\\ \times&0\\ \times&\times\end{pmatrix},\ C_5:\begin{pmatrix}\times&0\\ \times&\times\\ \times&0\end{pmatrix},\ C_6:\begin{pmatrix}\times&\times\\ \times&0\\ \times&0\end{pmatrix}. \end{aligned} \quad (23)$$

Applying the seesaw formula in Eq. (10) to the possible R_i and B_i and C_i textures, we may immediately infer that any combination of the cases R_i and C_j, and R_4 and B_j, with $i=1,\cdots,4$ and $j=1,\cdots,6$, are excluded since one of the mixing angles is predicted to be zero. Following the notation of [13], we classify the obtained $\mathbf{M}^\nu$ of the remaining structures R_i and B_j, with $i=1,\cdots,3$ and $j=1,\cdots,6$, into the following classes

$$\begin{aligned} &A:\begin{pmatrix}0&\times&\times\\ \times&\times&\times\\ \times&\times&\times\end{pmatrix},\ B:\begin{pmatrix}\times&0&\times\\ 0&\times&\times\\ \times&\times&\times\end{pmatrix},\ C:\begin{pmatrix}\times&\times&0\\ \times&\times&\times\\ 0&\times&\times\end{pmatrix},\\ &D:\begin{pmatrix}\times&\times&\times\\ \times&0&\times\\ \times&\times&\times\end{pmatrix},\ E:\begin{pmatrix}\times&\times&\times\\ \times&\times&0\\ \times&0&\times\end{pmatrix},\ F:\begin{pmatrix}\times&\times&\times\\ \times&\times&\times\\ \times&\times&0\end{pmatrix}. \end{aligned} \quad (24)$$

The classes B, C and E are obtained from the textures R_1 and B_1 or B_4, B_2 or B_5, and B_3 or B_6, respectively. The classes A, D and F are generated through R_2 (R_3) and the cases B_1 or B_2 (B_4 or B_5), B_3 or B_4 (B_1 or B_6), and B_5 or B_6 (B_2 or B_3), respectively.

Three (or more) texture zeros are automatically excluded since they lead to two (or more) vanishing neutrino mixing angles [14]. Thus, the minimal version of the type I seesaw model is given by the 2RHN model assuming two texture zeros in the neutrino Dirac mass matrix.

B. Predictions from the Maximally Restrictive 2RHN model

We may now look for the pairs of $\mathbf{M_R}$ (with one or two zeros) and $\mathbf{Y}^\nu$ (with the maximal number of zeros) which are compatible with observations, at least, at 3σ C.L.. For that purpose, we analyse the consequences of such constraints in the effective neutrino mass matrix $\mathbf{M}^\nu$. From Eq. (11),

$$\mathbf{M}^\nu_{\alpha\beta}=\sum_i m_i \mathbf{O}^*_{\alpha i}\mathbf{O}^*_{\beta i}, \quad (25)$$

where $\mathbf{O}=\mathrm{diag}(e^{i\delta_e},e^{i\delta_\mu},e^{i\tau})\mathbf{U}\mathrm{diag}(e^{-i\varphi_1},e^{-i\varphi_1},1)$ is the most general matrix that diagonalises $\mathbf{M}^\nu$, before the rephasing of the charged fields and considering the presence of the unphysical Majorana phase [15]. In order to test the compatibility of the one-zero textures in Eq. (24), one has to test the validity of $\mathbf{M}^\nu_{\alpha\beta}=0$, which translates into

$$\text{NH: } \frac{m_2}{m_3}=-\frac{\mathbf{O}^*_{\alpha3}\mathbf{O}^*_{\beta3}}{\mathbf{O}^*_{\alpha2}\mathbf{O}^*_{\beta2}},\quad \text{IH: } \frac{m_1}{m_2}=-\frac{\mathbf{O}^*_{\alpha2}\mathbf{O}^*_{\beta2}}{\mathbf{O}^*_{\alpha1}\mathbf{O}^*_{\beta1}}. \quad (26)$$

Taking the absolute value of the above expressions, one may test the validity of the resulting conditions for the light-neutrino mass ratio. Scanning over the mixing angles 1 and 3σ intervals (see Table I) and the interval $[0,2\pi[$ for δ, we conclude that the compatible $\mathbf{M}^\nu$ textures with neutrino data at 1σ are B and C for IH, and the ones compatible at 3σ are D and F also for IH. The δ and α predictions for each texture are presented in Fig. 1. The predicted δ phases for the cases B and C are extremely close to its current best-fit value presented in Table I. On the other hand, the results for D and F are more disperse, and the predicted δ is out of its 1σ experimental range. Our results are compatible with the ones obtained in [16].

To complete our analysis, we verify if some of the textures that were proved to be experimentally excluded become compatible with the data in the basis where $\mathbf{Y}^\ell$ is non-diagonal, with six zeros. In those cases the matrix $\mathbf{U}^{\ell*}_\mathbf{L}$ is a permutation matrix. Thus, rotating on the left the unviable structures in the charged-lepton mass basis by $\mathbf{U}^{\ell\ *}_\mathbf{L}$ we find that textures A and E become valid. The $\mathbf{M}^\nu$ textures generated from C_i for IH, and B_i and C_i for NH remain invalid since any row permutation can lead them to a valid case.

With the goal of constructing a more predictive model, we may assume that, beyond the considered texture ze-

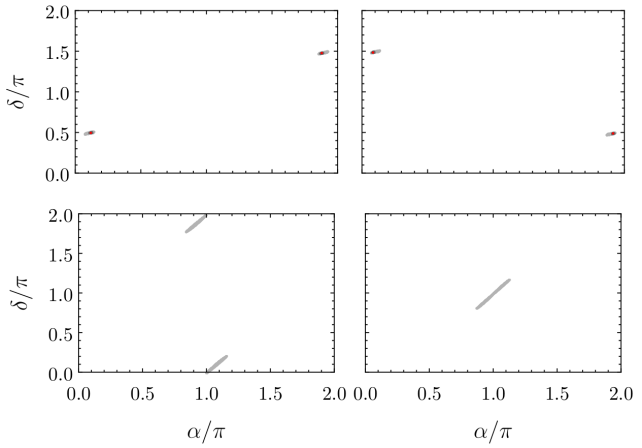

Figure 1. Predictions for α and δ for textures B (top left), C (top right), D (bottom left) and F (bottom right) valid at the interval 1σ (dark-grey points) and 3σ (light-grey points). The red points correspond to the predictions computed using the best-fit values in Table I.

ros, some of the $\mathbf{Y}^\nu$ elements are equal. This assumption leads to correlations among the elements of $\mathbf{M}^\nu$. In the case of textures B and C, if we consider that three $\mathbf{Y}^\nu$ elements are equal, then two components of $\mathbf{M}^\nu$ will be the same, meaning $\mathbf{M}^\nu_{\alpha\beta} = \mathbf{M}^\nu_{\sigma\rho}$, and

$$\frac{m_1}{m_2} = \frac{\mathbf{O}^*_{\sigma 2}\mathbf{O}^*_{\rho 2} - \mathbf{O}^*_{\alpha 2}\mathbf{O}^*_{\beta 2}}{\mathbf{O}^*_{\alpha 1}\mathbf{O}^*_{\beta 1} - \mathbf{O}^*_{\sigma 1}\mathbf{O}^*_{\rho 1}}, \tag{27}$$

for IH. Moreover, the ratio M_2/M_1 is fixed by the remaining correlations in $\mathbf{M}^\nu$. Analysing the compatibility of this expression, taking into account the conditions for δ and α obtained from the valid zero relations, we conclude that for B, the textures B_1 with $\mathbf{Y}^\nu_{21} = \mathbf{Y}^\nu_{31} = \mathbf{Y}^\nu_{32}$ and $\mathbf{Y}^\nu_{21} = \mathbf{Y}^\nu_{31} = \mathbf{Y}^\nu_{12}$ are valid, and all their $2-3$ row permutations (texture C) or column permutations followed by row and column permutation in R_1 (remaining structures in texture B), are valid up to 3σ C.L.. No D or C texture remains valid after considering the equality among three elements of $\mathbf{Y}^\nu$. Therefore, for these cases we decrease the number of constrains and consider that only two $\mathbf{Y}^\nu$ elements are the same. In this case, the resulting $\mathbf{M}^\nu$ matrices have either two equal elements with unfixed M_2/M_1, or no equality between its elements, but correlations among them that fix M_2/M_1. We proceed the same way as before, and verify if (under the one-zero predictions) the arising relations remain valid. We concluded that the following structures remain valid up to 3σ for the texture D with the $\mathbf{M_R}$ structure R_3: B_1 with $\mathbf{Y}^\nu_{31} = \mathbf{Y}^\nu_{32}$, $\mathbf{Y}^\nu_{21} = \mathbf{Y}^\nu_{32}$, $\mathbf{Y}^\nu_{31} = \mathbf{Y}^\nu_{32}$ or $\mathbf{Y}^\nu_{21} = \mathbf{Y}^\nu_{12}$; and for the texture F with the $\mathbf{M_R}$ structure R_3: B_3 with $\mathbf{Y}^\nu_{11} = \mathbf{Y}^\nu_{22}$, $\mathbf{Y}^\nu_{11} = \mathbf{Y}^\nu_{12}$, $\mathbf{Y}^\nu_{31} = \mathbf{Y}^\nu_{22}$ or $\mathbf{Y}^\nu_{31} = \mathbf{Y}^\nu_{12}$. All the other viable textures may be obtained by $2-3$ row permutations in $\mathbf{Y}^\nu$, or by column permutations in $\mathbf{Y}^\nu$ followed by row and column permutation in $\mathbf{M_R}$.

In order to verify the validity of our results and to extract predictions for the phases δ and α, and also for the ratio M_2/M_1 (in the more restricted cases), we performed a χ^2-analysis. With the purpose of finding the minimal χ^2 for a certain range of input parameters of our model (the structures of $\mathbf{Y}^\nu$ and $\mathbf{M_R}$) we used the MINUIT package [17], in a Fortran routine. We include six observables in our analysis: θ_{13}, θ_{12}, θ_{23}, Δm^2_{21}, Δm^2_{31} and δ with the best-fit values and respective errors at 1σ and 3σ depicted in Table I. The phase α is obviously not included in the fit because it was not measured so far. We will consider as well that δ is an unconstrained prediction of our model, since it is poorly measured and its χ^2 is not able to affect drastically the final result. The low-energy predictions corresponding to each one of the obtained valid cases are depicted in Table III. When correlations among the $\mathbf{M}^\nu$ components are considered, we get the results of Table IV, for the valid $\mathbf{M}^\nu$.

Structure			**Low-Energy Predictions**					
$\mathbf{M}^\nu$	$\mathbf{M_R}$	$\mathbf{Y}^\nu$	$\chi^2_{\min}$	δ/π	α/π	$m_{\beta\beta}$	J_{CP}	C.L.
B	R_1	B_1, B_4	0.037	1.49	1.88	4.78	16.37	1σ
C	R_1	B_2, B_5	0.025	1.50	0.08	4.82	16.38	1σ
D	R_2	B_3, B_4	0.747	1.96	0.97	1.65	1.88	3σ
	R_3	B_1, B_6						
F	R_2	B_5, B_6	1.896	1.05	1.04	1.65	2.78	3σ
	R_3	B_2, B_3						

Table III. Viable textures for $\mathbf{M_R}$ and $\mathbf{Y}^\nu$ and corresponding MINUIT predictions for δ, α, the effective electron neutrino mass $m_{\beta\beta} = |\mathbf{M}^\nu_{11}|$ in units of 10^{-2} eV, and the invariant $J_{CP} = s_{12}c_{12}s_{23}c_{23}s_{13}c_{13}\sin\delta$ in units of 10^{-3}, for IH. The minimal χ^2 for the obtained low-energy predictions is also presented.

Structure			**Predictions**				
$\mathbf{M}^\nu$	$\mathbf{M_R}$	$\mathbf{Y}^\nu$	M_2/M_1	$\chi^2_{\min}$	δ/π	α/π	C.L.
B	R_1	$B_1 : \mathbf{Y}^\nu_{21} = \mathbf{Y}^\nu_{31} = \mathbf{Y}^\nu_{32}$	1.90	0.203	1.50	1.90	3σ
		$B_1 : \mathbf{Y}^\nu_{21} = \mathbf{Y}^\nu_{31} = \mathbf{Y}^\nu_{12}$	11.78				
C		$B_2 : \mathbf{Y}^\nu_{21} = \mathbf{Y}^\nu_{31} = \mathbf{Y}^\nu_{12}$	1.90	0.202	1.50	0.10	3σ
		$B_2 : \mathbf{Y}^\nu_{21} = \mathbf{Y}^\nu_{31} = \mathbf{Y}^\nu_{22}$	11.78				
D	R_3	$B_1 : \mathbf{Y}^\nu_{31} = \mathbf{Y}^\nu_{32}$	1.10	0.747	1.96	0.97	3σ
		$B_1 : \mathbf{Y}^\nu_{21} = \mathbf{Y}^\nu_{32}$	1.13				
		$B_1 : \mathbf{Y}^\nu_{31} = \mathbf{Y}^\nu_{12}$	1.53				
		$B_1 : \mathbf{Y}^\nu_{21} = \mathbf{Y}^\nu_{12}$	1.68				
F		$B_3 : \mathbf{Y}^\nu_{11} = \mathbf{Y}^\nu_{22}$	1.57	1.896	1.05	1.04	3σ
		$B_3 : \mathbf{Y}^\nu_{11} = \mathbf{Y}^\nu_{12}$	5.41				
		$B_3 : \mathbf{Y}^\nu_{31} = \mathbf{Y}^\nu_{22}$	7.31				
		$B_3 : \mathbf{Y}^\nu_{31} = \mathbf{Y}^\nu_{12}$	97.95				

Table IV. Maximally restrictive viable cases for two (textures D and F) or three (textures B and C) equal elements in $\mathbf{Y}^\nu$ and the corresponding MINUIT predictions for δ and α, for IH. The minimal χ^2 is also presented. The remaining valid cases may be obtained by the appropriate column and (or) row permutation of $\mathbf{M_R}$ (and) or $\mathbf{Y}^\nu$.

IV. Type I Seesaw Leptogenesis

The baryon asymmetry may be defined through the baryon-to-photon ratio given by

$$\eta_B \equiv \frac{n_B - n_{\bar{B}}}{n_\gamma} \,, \tag{28}$$

where n_B, $n_{\bar{B}}$ are the number densities of baryons and anti-baryons, respectively, and n_γ is the number density of photons. The present value of the baryon-to-photon ratio, from the combined data of nine-year WMAP observations, Supernova Legacy Survey three year sample and Baryonic Acoustic Oscillations [18], is

$$\eta_B^0 = (6.16 \pm 0.12) \times 10^{-10} \,. \tag{29}$$

In the modern theory of baryogenesis, the mechanism that generates a baryon asymmetry in the exact quantity observed today is not known. However, in a qualitative way, one knows that the asymmetry must have been generated dynamically from a symmetric state, due to inflation. Therefore, there must have been a mechanism that was able per se to generate an asymmetric state from the symmetric one. In 1967, Sakharov [19] concluded that three requirements were necessary to generate such asymmetry: baryon number (B) violation; C and CP violation; and departure from thermal equilibrium. In spite of enclosing all three Sakharov conditions, the SM underestimates the baryon asymmetry. Thus, one needs to go beyond the SM, in order to find new sources of CP violation and other ways to promote departure from equilibrium.

From the models that can explain baryogenesis, one of the simplest and well-motivated scenarios is leptogenesis [20], where the generated asymmetry comes from the out-of-equilibrium decays of heavy fermions or bosons involving leptons. Such interactions in the early Universe are also the ones relevant for the smallness of neutrino masses through the seesaw mechanism, as previously seen. Leptogenesis accounts naturally for the three Sakharov conditions: seesaw interactions naturally break lepton number (L) (and, hence, baryon number, together with $(B+L)$-violating sphaleron processes) due to the Majorana character of neutrinos; also, CP violation is present in the heavy-particle interactions due to the complex character of Yukawa couplings; finally, leptogenesis predicts that the decay of the new bosons or fermions is out of equilibrium due to their large masses and to the rapid expansion of the Universe in the early times. The generated baryon asymmetry may be written generally as the product of three factors, $\eta_B = d\,\epsilon\,\kappa$, where d accounts for the redistribution of the leptonic asymmetry to other particle species, ϵ is the CP asymmetry generated in the heavy-particle decays, and κ is an efficiency factor that accounts for washout factors that suppress the previously-generated asymmetry.

The generated lepton asymmetry in the decay of heavy neutrinos is partially converted into a baryon asymmetry through $(B+L)$-violating sphaleron processes. That conversion may be quantified as $B/(B-L) = 28/79 \equiv a_{\rm sph}$ [21]. Thus, in terms of the present baryon-to-photon ratio, one has

$$\eta_B = a_{\rm sph}\,\frac{N^{\rm f}_{B-L}}{N^{\rm rec}_\gamma} \sim 9.58 \times 10^{-3}\, N^{\rm f}_{B-L} \,, \tag{30}$$

where $N^{\rm f}_{B-L}$ is the final asymmetry calculated in a portion of comoving volume and $N^{\rm rec}_\gamma$ is the number of photons in the same portion of comoving volume (~ 37.01) at the recombination temperature. The $N^{\rm f}_{B-L}$ computation depends on the considered temperature regime.

The second ingredient, the CP asymmetry, may be computed as

$$\epsilon_i^\alpha = \frac{\Gamma(N_i \to \Phi \ell_\alpha) - \Gamma(N_i \to \Phi^\dagger \bar{\ell}_\alpha)}{\sum_\beta [\Gamma(N_i \to \Phi \ell_\beta) + \Gamma(N_i \to \Phi^\dagger \bar{\ell}_\beta)]}, \tag{31}$$

where $\Gamma(N_i \to \Phi \ell_\alpha) \equiv \Gamma_i^\alpha$ and $\Gamma(N_i \to \Phi^\dagger \bar{\ell}_\alpha) \equiv \overline{\Gamma}_i^\alpha$ are the N_i decay widths into the lepton doublets ℓ_α and antileptons $\bar{\ell}_\alpha$, respectively, and the Higgs doublet Φ, and the sum in the denominator runs over the three lepton flavours. At tree level, the total flavoured decay rate difference is zero, as

$$\Gamma_i^\alpha = \overline{\Gamma}_i^\alpha = M_i \frac{|\mathbf{Y}^\nu_{\alpha i}|^2}{16\pi} \,, \tag{32}$$

and no CP asymmetry is generated. Hence, the first non-zero contribution to the asymmetry ϵ_i^α must arise from the interference of the tree-level process with its one-loop corrections [22] (vertex and self-energy, in Fig. 2). The resultant CP asymmetry reads

$$\epsilon_i^\alpha = \frac{1}{8\pi}\frac{1}{\mathbf{H}^\nu_{ii}} \{ {\rm Im}[\mathbf{Y}^{\nu *}_{\alpha i} \mathbf{H}^\nu_{ij} \mathbf{Y}^\nu_{\alpha j}][f(x_j) + g(x_j)] + \\ + {\rm Im}[\mathbf{Y}^{\nu *}_{\alpha i} \mathbf{H}^\nu_{ji} \mathbf{Y}^\nu_{\alpha j}] g'(x_j) \} \,, \tag{33}$$

for $i \neq j$, where $x_j = M_j^2/M_i^2$ and $f(x)$, $g(x)$ and $g'(x)$ are the one-loop vertex and wave functions,

$$f(x) = \sqrt{x}\left[1 - (1+x)\ln\left(1 + \frac{1}{x}\right)\right], \tag{34}$$

$$g(x) = \sqrt{x} g'(x) = -\frac{\sqrt{x}}{(x-1)}. \tag{35}$$

Furthermore, the unflavoured CP asymmetry is obtained by summing over flavour the asymmetry in Eq. (33),

$$\epsilon_i = \frac{1}{8\pi}\frac{1}{\mathbf{H}^\nu_{ii}} \sum_{j \neq i} {\rm Im}[(\mathbf{H}^\nu_{ij})^2][f(x_j) + g(x_j)] \,. \tag{36}$$

We may parametrise the washout of the N_i density using the decay parameter K for the flavour channel α

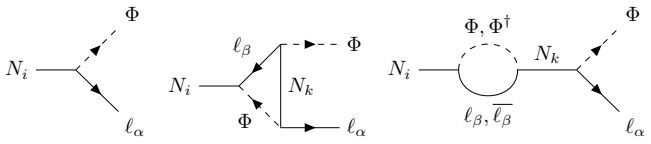

Figure 2. Heavy-neutrino decay diagrams. The first diagram, corresponds to the tree-level contribution while the second and third diagrams are its one-loop vertex and self-energy corrections, respectively.

as

$$K_i^\alpha = \frac{\Gamma_{\mathrm{D}i}{}^\alpha(T \gg M_i)}{H(M_i)} \equiv \frac{\tilde{m}_i^\alpha}{m_*} \,, \tag{37}$$

where $\Gamma_{\mathrm{D}i}{}^\alpha$ denotes the tree-level flavoured decay width defined in Eq. (32), $H(T)$ is the Universe expansion rate, $\tilde{m}_i^\alpha$ is the flavoured effective neutrino mass given by

$$\tilde{m}_i^\alpha = \frac{v^2 |\mathbf{Y}^\nu_{\alpha i}|^2}{M_i}, \tag{38}$$

and $m_* \simeq 1.09 \times 10^{-3}$ eV is the equilibrium neutrino mass. Summing over flavour, one obtains the total decay parameter, $K_i = \sum_\alpha K_i^\alpha = \tilde{m}_i/m_*$, where $\tilde{m}_i$ is the effective neutrino mass given by

$$\tilde{m}_i = \sum_\alpha \tilde{m}_i^\alpha = \frac{v^2\, \mathbf{H}^\nu_{ii}}{M_i} \,. \tag{39}$$

The relation between $\tilde{m}_i$ and m_* is a measure of thermal equilibrium for the decays, i. e., it shows if the asymmetry is strongly ($\tilde{m}_i \gg m_*$) or weakly ($\tilde{m}_i \ll m_*$) washed out by inverse decays. The way washout processes modify the L-asymmetry is parametrised by the efficiency factor κ, which is obtained by solving the Boltzmann Equations (BEs) for the considered system. In this work we consider the contribution of both neutrinos N_1 and N_2 for the final asymmetry because we are interested in analysing the case of $M_2 \gtrsim 3M_1$. Since we are in thermal leptogenesis and in a relatively strong hierarchy for the heavy-neutrino masses, $N_{N_1}(T \sim M_2) \simeq N_{N_2}(T \sim M_1) \simeq 0$ is verified and we may divide our analysis into two distinct phases: the N_1 and the N_2 leptogenesis. Furthermore, we will consider a "strong-coupling N_1 scenario", where part of the lepton asymmetry generated by N_2 decays is projected onto a flavour-direction protected against washout from N_1 interactions.

For temperatures above 10^{12} GeV (unflavoured regime) in the early Universe, the charged lepton Yukawa interactions are out of equilibrium. Hence, for this temperature range, the three lepton doublets will be indistinguishable, and its lepton asymmetry may be represented rigorously by a single mass eigenstate:

$$|\ell_i\rangle = \sum_\alpha c_i^\alpha |\ell_\alpha\rangle \quad \text{and} \quad |\bar{\ell}_i\rangle = \sum_\alpha \bar{c}_i^\alpha |\bar{\ell}_\alpha\rangle \,, \tag{40}$$

for a decay $N_i \to \Phi \ell_i$ and its CP-conjugate $N_i \to \Phi^\dagger \bar{\ell}_i$, respectively, with $\alpha = e, \mu, \tau$ and $i = 1, 2$. The total lepton-number asymmetry is the important quantity, and its evolution may be tracked with a single BE. To describe the $(B-L)$-asymmetry evolution in this regime, we will follow [23]. In this temperature regime we consider that the processes that affect the evolution N_{B-L} are the N_i out-of-equilibrium decays, inverse decays and $\Delta L = 1$ scatterings involving the top quark.

To adress this problem we used the approximate analytic solutions to the efficiency factor $\kappa_i(K_i)$ obtained in [23]. The $(B-L)$-asymmetry is computed through

$$N^f_{B-L} \simeq -\epsilon_1 \kappa_1 - \left(1 - P_{21} + P_{21} e^{\frac{3\pi K_1}{8}}\right) \epsilon_2 \kappa_2 \,, \tag{41}$$

where ϵ_i are given by Eq. (36) and P_{21} is the probability that the lepton asymmetry generated in the N_2 leptogenesis is projected onto the flavour direction of the asymmetry generated in the N_1 interactions. The $(B-L)$-asymmetry is then transformed into the baryon-to-photon ratio through Eq. (30). Note that for a successful baryogenesis, able to reproduce Eq. (29), and for the typical values $\kappa \sim 0.1$, the produced CP asymmetry must be at least of the order of 10^{-6}.

In order to study leptogenesis at lower temperatures, in the interval 10^9 GeV $\ll T \ll 10^{12}$ GeV (flavoured regime), we must consider a two-flavour lepton evolution regime. Hence, processes involving leptons are able to distinguish between two different lepton-doublet flavours: the τ flavour, $|\ell_\tau\rangle$, and a coherent superposition of the e and μ flavours, $|\ell_\gamma\rangle$. To solve this problem, one must define the new flavoured asymmetry $\Delta_\alpha \equiv B/3 - L_\alpha$. The final $(B-L)$-asymmetry, obtained by solving the flavour dependent BEs, is the sum of all the obtained Δ_α asymmetries.

Once again, a numerical treatment is required to find the BEs solutions. This time we used the analytical approximations of the numerical solutions for the flavoured efficiency factors κ_i^α presented in [24], where only N_i decays and inverse decays are taken into account. In the temperature range we are interested in, there are only two statistically independent lepton flavours when N_2 leptogenesis occurs: τ, and a coherent combination of the e and μ flavours, γ_2, generated by N_2 decays. When N_1 processes start to be active, the previously obtained flavour state $|\ell_{\gamma_2}\rangle$ is no longer able to participate in the N_1 decays and inverse decays as a coherent state. Under the action of N_1, the flavour states generated by N_2 will be an incoherent superposition of two new flavour states: the orthogonal component to $|\ell_1\rangle$, $|\ell_{\gamma_1^\perp}\rangle$, and the parallel component to $|\ell_1\rangle$, $|\ell_{\gamma_1}\rangle$. Effectively, the system is now in a tree-flavour regime: the τ flavour, still out of equilibrium, and the two new independent components γ_1 and $\gamma_1^\perp$. Only the τ and γ_1 flavour asymmetries are affected by the decays and inverse decays of N_1. The component $\gamma_1^\perp$ is orthogonal to the interaction channels of N_1, remaining inert. Thus, the approximate analytical

solutions for the final asymmetries, may be written as

$$N^f_{\Delta_{\gamma_1}} \simeq -P_{\gamma_2\gamma_1}\,\epsilon^\gamma_2\,\kappa^\gamma_2\,e^{-\frac{3\pi}{8}K^\gamma_1} - \epsilon^\gamma_1\,\kappa^\gamma_1\,, \tag{42}$$

$$N^f_{\Delta_\tau} \simeq -\epsilon^\tau_2\,\kappa^\tau_2\,e^{-\frac{3\pi}{8}K^\tau_1} - \epsilon^\tau_1\,\kappa^\tau_1\,, \tag{43}$$

$$N^f_{\Delta_{\gamma_1^\perp}} \simeq -\left(1-P_{\gamma_2\gamma_1}\right)\epsilon^\gamma_2\,\kappa^\gamma_2\,, \tag{44}$$

where $P_{\gamma_2\gamma_1}$ is the probability of flavour γ_2 to be transformed into γ_1. The final $(B-L)$-asymmetry is then computed by summing the three individual asymmetries:

$$N^f_{B-L} = N^f_{\Delta_{\gamma_1}} + N^f_{\Delta_{\gamma_1^\perp}} + N^f_{\Delta_\tau}, \tag{45}$$

and the final η_B is computed through Eq. (30).

V. Leptogenesis in the Maximally Restrictive Type I Seesaw Model

We can now express the CP asymmetries and efficiency factors obtained in the last section as functions of the z parameter in Eq. (16), and calculate η_B. For each $\mathbf{Y}^\nu$ texture zero we will obtain expressions of this quantity uniquely as a function of low-energy parameters and heavy-neutrino masses. The second zero will fix the Dirac and Majorana phases.

A. Predictions for the Flavoured Regime

In order to obtain the $(B-L)$-asymmetry we have to compute the CP asymmetries and efficiency factors for each flavour. The dependence of these quantities on the low-energy parameters can be obtained expressing the elements of $\mathbf{Y}^\nu$ in terms of the Casas-Ibarra parametrisation in Eq. (15), in the basis where both $\mathbf{Y}^\ell$ and $\mathbf{M_R}$ are diagonal.

As a function of the z parameter (for IH), for each one of the contributions from N_1 and N_2, the CP asymmetry in Eq. (33) may be written as

$$\epsilon^\alpha_1 = -\frac{1}{8\pi v^2}\frac{M_2}{m_1|\cos z|^2 + m_2|\sin z|^2}\{A^\alpha_1\left[f\left(x_2\right)+g\left(x_2\right)\right] + B^\alpha_1 g'\left(x_2\right)\}\,, \tag{46}$$

$$\epsilon^\alpha_2 = -\frac{1}{8\pi v^2}\frac{M_1}{m_1|\sin z|^2 + m_2|\cos z|^2}\{A^\alpha_2\left[f\left(x_1\right)+g\left(x_1\right)\right] + B^\alpha_2 g'\left(x_1\right)\}\,, \tag{47}$$

where the factors $A^\alpha_{1(2)}$ and $B^\alpha_{1(2)}$ are functions of z, the masses m_1 and m_2 and $\mathbf{U}$.

To proceed, we replace the expressions for $\tan z$, shown in Table II, in Eqs. (46) and (47), for each valid texture-zero structure (for the cases R_1, R_2 and R_3, see Section III). It turns out, the CP asymmetries obtained numerically for the low-energy phases predicted bay the considered texture zeros, are well below the required minimum asymmetry ($\sim 10^{-7}$) for the maximal efficiency factor value (~ 1). We fix the heavy-neutrino masses close to the maximum value allowed in the considered regime ($M_1 = 10^{11}$ GeV and $M_2 = 3\times10^{11}$ GeV). This is justified by the fact that the CP asymmetry grows monotonously with the mass M_1. The obtained $|\epsilon^\alpha_i|$ values are compiled in Table V, where we show that all values lay in the range 10^{-11} to 10^{-8}. Thus, we conclude that none of the cases is able to produce a sufficiently high CP asymmetry to reproduce the present BAU. This conclusion is numerically confirmed by explicit computation of the final asymmetry using Eq. (45).

$\mathbf{M_R}$	$\mathbf{Y}^\nu$	**Flavoured CP asymmetries**			
		ϵ^γ_1 $(\times10^{-8})$	ϵ^τ_1 $(\times10^{-8})$	ϵ^γ_2 $(\times10^{-8})$	ϵ^τ_2 $(\times10^{-8})$
R_1	B_1	0.013	−2.500	−0.013	0.238
	B_2	1.980	−0.213	−0.383	0.223
	B_4	−0.013	2.511	0.013	−0.236
	B_5	−1.992	0.215	0.380	−0.221
R_2	B_4	−1.191	−0.276	0.592	−0.460
	B_5	0.046	2.124	0.767	−0.960
	B_3	−0.676	0.118	−0.008	0.059
	B_6	0.485	0.0216	0.464	−0.511
R_3	B_1	−0.826	−0.263	0.464	−0.367
	B_2	−0.072	1.671	0.511	−0.653
	B_3	0.726	1.362	1.262	1.453
	B_6	−1.381	−0.042	0.150	−0.021

Table V. ϵ^α_i for each texture-zero compatible with neutrino data. These values were obtained for the low-energy data in Table I, $M_1 = 10^{11}$ GeV and $M_2 = 3\times10^{11}$ GeV and for δ and α in Table III.

B. Predictions for the Unflavoured Regime

As discussed in Section IV, the final asymmetry for this case is uniquely determined by the asymmetries ϵ_1, ϵ_2, the efficiency factors κ_1, κ_2 and the probability P_{21}.

The expression for the unflavoured CP asymmetry in Eq. (36) may be written as well in terms of the Casas-Ibarra parametrisation. Replacing the elements of the corresponding matrix $\mathbf{R}$, one has

$$\epsilon_1 = -\frac{M_2}{8\pi v^2}\frac{(m_2^2-m_1^2)\,\mathrm{Im}[\sin^2 z]}{m_1\,|\cos z|^2 + m_2\,|\sin z|^2}\left[f\left(x_2\right)+g\left(x_2\right)\right], \tag{48}$$

$$\epsilon_2 = -\frac{M_1}{8\pi v^2}\frac{(m_2^2-m_1^2)\,\mathrm{Im}[\cos^2 z]}{m_1\,|\sin z|^2 + m_2\,|\cos z|^2}\left[f\left(x_1\right)+g\left(x_1\right)\right]. \tag{49}$$

To proceed, we replace the expressions for $\tan z$, shown in Table II, in Eqs. (48) and (49), for each valid texture-zero structure (for the cases R_1, R_2 and R_3, see Section III). This time, the CP asymmetries numerically obtained, for the low-energy phases predicted by the considered texture zeros, are within the required values to predict a correct baryon asymmetry. Combining the results ob-

$\mathbf{M_R}$	$\mathbf{Y}^\nu$	ϵ_1 $(\times 10^{-5})$	ϵ_2 $(\times 10^{-5})$	κ_1 $(\times 10^{-3})$	κ_2 $(\times 10^{-3})$	M_1 $(\times 10^{13}$ GeV)
R_1	B_1	-1.67	0.06	4.024	4.049	7.3
	B_5	-1.58	0.08	4.084	4.058	10.3
R_2	B_4	-3.02	0.44	2.278	2.300	33.8
	B_3	-6.31	4.03	1.076	1.071	125.0
R_3	B_1	-4.83	2.02	1.385	1.377	76.0
	B_6	-3.35	0.90	1.952	1.968	49.0

Table VI. ϵ_i, κ_i and N_1 mass values that generate the $\eta_{\rm B}$ best-fit value in Eq. (29), for each compatible texture. These results are obtained using the low-energy parameters that guarantee the minimum χ^2 value in Table III, and $M_2 = 10^{16}$ GeV.

$\mathbf{M_R}$	$\mathbf{Y}^\nu$	ϵ_1 $(\times 10^{-5})$	ϵ_2 $(\times 10^{-5})$	κ_1 $(\times 10^{-3})$	κ_2 $(\times 10^{-3})$	M_1
R_1	$B_1 : \mathbf{Y}^\nu_{21} = \mathbf{Y}^\nu_{31} = \mathbf{Y}^\nu_{12}$	-1.40	-0.17	4.113	4.139	0.59
	$B_1 : \mathbf{Y}^\nu_{21} = \mathbf{Y}^\nu_{31} = \mathbf{Y}^\nu_{32}$	-1.89	0.32	4.113	4.139	0.97
	$B_5 : \mathbf{Y}^\nu_{22} = \mathbf{Y}^\nu_{32} = \mathbf{Y}^\nu_{11}$	-1.39	-0.17	4.139	4.113	0.58
	$B_5 : \mathbf{Y}^\nu_{22} = \mathbf{Y}^\nu_{32} = \mathbf{Y}^\nu_{21}$	-1.87	0.32	4.139	4.113	0.95
R_2	$B_3 : \mathbf{Y}^\nu_{31} = \mathbf{Y}^\nu_{12}$	-27.39	29.32	0.2378	0.238	51.70
	$B_3 : \mathbf{Y}^\nu_{11} = \mathbf{Y}^\nu_{12}$	-8.18	6.94	0.833	0.829	15.40
	$B_3 : \mathbf{Y}^\nu_{31} = \mathbf{Y}^\nu_{22}$	-7.39	5.26	0.921	0.917	13.80
	$B_3 : \mathbf{Y}^\nu_{11} = \mathbf{Y}^\nu_{22}$	-5.43	0.74	1.211	1.204	9.81
	$B_6 : \mathbf{Y}^\nu_{21} = \mathbf{Y}^\nu_{12}$	-1.33	-0.39	3.870	3.930	1.37
R_3	$B_1 : \mathbf{Y}^\nu_{31} = \mathbf{Y}^\nu_{12}$	-0.98	-0.12	4.135	4.066	5.15
	$B_1 : \mathbf{Y}^\nu_{21} = \mathbf{Y}^\nu_{12}$	-1.41	-0.29	3.897	3.835	2.34
	$B_2 : \mathbf{Y}^\nu_{21} = \mathbf{Y}^\nu_{22}$	-2.45	-1.78	1.940	1.924	0.61
	$B_2 : \mathbf{Y}^\nu_{31} = \mathbf{Y}^\nu_{22}$	-2.07	-1.51	2.447	2.421	0.40
	$B_6 : \mathbf{Y}^\nu_{11} = \mathbf{Y}^\nu_{32}$	-14.90	15.97	0.443	0.444	32.70
	$B_6 : \mathbf{Y}^\nu_{11} = \mathbf{Y}^\nu_{12}$	-4.75	2.84	1.515	1.526	8.90
	$B_6 : \mathbf{Y}^\nu_{21} = \mathbf{Y}^\nu_{32}$	-4.32	2.15	1.665	1.678	7.69
	$B_6 : \mathbf{Y}^\nu_{12} = \mathbf{Y}^\nu_{22}$	-3.11	0.25	2.135	2.155	3.86

Table VII. ϵ_i, κ_i and N_1 mass values ($\times 10^{14}$ GeV) that generate the $\eta_{\rm B}$ best-fit value in Eq. (29), for each compatible texture with correlations in $\mathbf{M}^\nu$. These results are obtained using the low-energy parameters that guarantee the minimum χ^2 value in Table IV and the respective M_2/M_1.

tained for the efficiency factors, through Eq. (41), we obtain the correct baryon-to-photon ratio for the Yukawa textures presented in Table VI, with the respective CP asymmetries, efficiency factors and the masses M_1, for $M_2 = 10^{16}$ GeV. Furthermore, for the maximally restrictive 2RHN model compatible with neutrino data (see Section III), where the ratio M_2/M_1 is fixed, the structures that account for the observed BAU, in Eq. (29), are presented in Table VII, for the mass hierarchies presented in Table IV.

VI. Concluding Remarks

In the present thesis we discussed the problem of neutrino mass generation in the framework of seesaw extensions to the SM. We focused our discussion on the maximally constrained 2RHN model. We concluded that, in the case of IH, some of the considered Dirac matrix patterns are indeed compatible with experimental data.

Having proved the compatibility of the maximally restrictive 2RHN mass model with current neutrino data, we discussed the consequences of adding two RH neutrinos to the SM for the origin of matter. Using the viable constraints found in Section III, we learned that some of those models are indeed compatible with the present experimental value of the BAU, for temperatures of above 10^{13} GeV in the early Universe.

Thus, we conclude that the considered model is not only compatible with neutrino data, but also succeeds in predicting the right value of the matter-antimatter asymmetry. The work developed in this thesis is a clear example of how a high-energy extension of the SM can provide solutions to both neutrino masses and the BAU, establishing a bridge between low-energy observations, obtained in the context of neutrino oscillations, and the origin of matter in the beginning of the Universe.

References

[1] N. Cabibbo, *Phys. Rev. Lett.* **10**, 531 (1963).
[2] M. Kobayashi, T. Maskawa, *Progress of Theoretical Physics* **49**, 652 (1973).
[3] Y. Fukuda, *et al.*, *Phys. Rev. Lett.* **81**, 1562 (1998).
[4] Q. R. Ahmad, *et al.*, *Phys. Rev. Lett.* **89**, 011301 (2002).
[5] S. Weinberg, *Phys. Rev. Lett.* **43**, 1566 (1979).
[6] A. Broncano, M. B. Gavela, E. E. Jenkins, *Phys. Lett. B* **552**, 177 (2003).
[7] B. Pontecorvo, *Sov. Phys. JETP* **6**, 429 (1957).
[8] Z. Maki, M. Nakagawa, S. Sakata, *Progress of Theoretical Physics* **28**, 870 (1962).
[9] C. Patrignani, *et al.*, *Chin. Phys. C* **40**, 100001 (2016).
[10] I. Esteban, M. C. Gonzalez-Garcia, M. Maltoni, I. Martinez-Soler, T. Schwetz, *Journal of High Energy Physics* **2017**, 87 (2017).
[11] J. A. Casas, A. Ibarra, *Nucl. Phys. B* **618**, 171 (2001).
[12] J. Zhang, S. Zhou, *JHEP* **09**, 065 (2015).
[13] Z.-z. Xing, *Phys. Rev. D* **69**, 013006 (2004).
[14] K. Harigaya, M. Ibe, T. T. Yanagida, *Phys. Rev. D* **86**, 013002 (2012).
[15] S. Antusch, J. Kersten, M. Lindner, M. Ratz, *Nucl. Phys. B* **674**, 401 (2003).
[16] R. R. Gautam, M. Singh, M. Gupta, *Phys. Rev. D* **92**, 013006 (2015).
[17] F. James, M. Roos, *Comput. Phys. Commun.* **10**, 343 (1975).
[18] G. Hinshaw, *et al.*, *The Astrophysical Journal Supplement Series* **208**, 19 (2013).
[19] A. D. Sakharov, *Pisma Zh. Eksp. Teor. Fiz.* **5**, 32 (1967).
[20] M. Fukugita, T. Yanagida, *Phys. Lett. B* **174**, 45 (1986).
[21] J. A. Harvey, M. S. Turner, *Phys. Rev. D* **42**, 3344 (1990).
[22] L. Covi, E. Roulet, F. Vissani, *Phys. Lett. B* **384**, 169 (1996).
[23] W. Buchmuller, P. Di Bari, M. Plumacher, *Nucl. Phys. B* **665**, 445 (2003).
[24] S. Antusch, P. Di Bari, D. A. Jones, S. F. King, *Phys. Rev. D* **86**, 023516 (2012).